Chapter 7

The Orthogonally Rotating Core in NGC 4698[1]

Abstract

The $R-$band isophotal map of the Sa galaxy NGC 4698 shows that the inner region of the bulge structure is elongated perpendicularly to the major axis of the disk, this is also true for the outer parts of the bulge if a parametric photometric decomposition is adopted. At the same time the stellar component is characterized by an inner velocity gradient and a central zero-velocity plateau along the minor and major axis of the disk respectively. This remarkable geometric and kinematic decoupling suggests that a second event occurred in the formation history of this galaxy.

7.1 Introduction

In the course of an investigation of the kinematic properties of early-type spiral galaxies we encountered the peculiar case of NGC 4698, which is the subject of this Chapter.

This galaxy is characterized by a remarkable geometric decoupling between bulge and disk, whose apparent major axes appear oriented in an orthogonal way at a simple visual inspection of the galaxy images (e.g., see Panels 78, 79 and 87 in Sandage & Bedke 1994). The stellar rotation curve exhibits an unusual zero-velocity plateau in the central portion of the disk major axis. A spectrum taken along the disk minor axis shows an inner velocity gradient of the stellar component suggesting the presence of a kinematic decoupling between the inner regions of the galaxy and its disk. This decoupling is a direct indication that distinct events occurred in the history of NGC 4698. For this reason it should be considered a noteworthy case for the interpretation of the processes leading to the formation of spirals.

NGC 4698 is classified Sa by Sandage & Tammann (1981) and Sab(s) by de Vaucouleurs et al. (1991, RC3). Sandage & Bedke (1994, CAG) in The Carnegie Atlas of Galaxies presented NGC 4698 in the Sa section as an example of the early-to-intermediate Sa type. They describe the galaxy as characterized by a large central E-like bulge in which there is no evidence of recent star formation or spiral structure. The spiral arms are tightly wound

[1]Bertola, F., Corsini, E. M., Vega Beltrán, J. C., Pizzella, A., Sarzi, M., Cappellari, M. & Funes, J. G. 1999, ApJ, 519, L127, expanded version

and become prominent only in the outer parts of the disk. They are defined primarily by the dust which forms fragmentary lanes of the multiple-armed type. NGC 4698 possesses all the characteristics of a spiral galaxy and therefore it is morphologically different from the ellipticals with polar ring, although in both cases we are facing a similar phenomenon of orthogonal geometric and kinematic decoupling (e.g. AM 2020-504 in Whitmore et al. 1990).

NGC 4698 belongs to the Virgo cluster. Its total $B-$band magnitude is $B_T = 11.46$ mag (RC3) which corresponds to $M_B = -19.69$ mag assuming a distance of 17 Mpc (Freedman et al. 1994).

7.2 Observations and data reduction

The photometric and spectroscopic observations of NGC 4698 were carried out with EFOSC2 at the ESO 3.6-m telescope in La Silla on March 1998, 20-21.

We obtained three 20-seconds images of the galaxy using the No. 40 Loral/Lesser 2048 $\times$ 2048 CCD with 15×15 μm^2 pixels in combination with the No. 642 $R-$band filter. It yielded an unvignetted field of view of $3\overset{'}{.}8 \times 5\overset{'}{.}3$ with an image scale of $0\overset{''}{.}32$ pixel^{-1} after an on-line binning of 2×2 pixels. The routine data reduction has been carried out using IRAF. Gaussian fit to the field stars in the final processed image yielded a point spread function FWHM $= 1\overset{''}{.}0$. The absolute calibration was made using the multi-aperture photometric data obtained in the same band by Schröeder & Visvanathan (1996) since no photometric standards were observed.

Two 30-minutes spectra were taken along the major (P.A. $= 170°$) and the minor axis (P.A. $= 80°$) of the galaxy. We used the No. 8 grism with 600 grooves mm^{-1} in combination with a $1\overset{''}{.}0 \times 5\overset{'}{.}7$ slit. The No. 40 CCD was adopted as detector. They yielded a wavelength coverage of 2048 Å between 4320 Å and 6368 Å with a reciprocal dispersion of 66.33 Å mm^{-1}. Each pixel of the spectra corresponds to 1.99 Å$\times\, 0\overset{''}{.}32$ after an on-line binning of 2×2 pixels. Comparison lamp exposures were obtained before and after each object integration. Some spectra of late-G or early-K giant stars were taken to serve as template in measuring the stellar kinematics. The seeing FWHM during the observing nights was between $1''$ and $1\overset{''}{.}5$ as measured by the Differential Image Motion Monitor of La Silla. Using standard MIDAS routines the spectra were bias subtracted, flat-field corrected, and wavelength calibrated. Cosmic rays were found and corrected by comparing the counts in each pixel with the local mean and standard deviation and substituting a suitable value. The instrumental resolution was derived by measuring the FWHM of a dozen of single emission lines distributed all over the spectral range of a calibrated comparison spectrum. It corresponds to a FWHM $= 6.41 \pm 0.07$ Å (i.e. $\sigma = 124$ km s^{-1} at Hα). The single spectra obtained along the same axis were aligned and co-added using their stellar-continuum centers as reference. In each spectrum the center of the galaxy was defined as the center of the Gaussian fitting the radial profile of the stellar continuum. The contribution of the sky was determined from the edges of the resulting frame and then subtracted. The stellar kinematics was measured from the spectra absorption lines using the Fourier Correlation Quotient Method (Bender 1990) as done by Bertola et al. (1996).

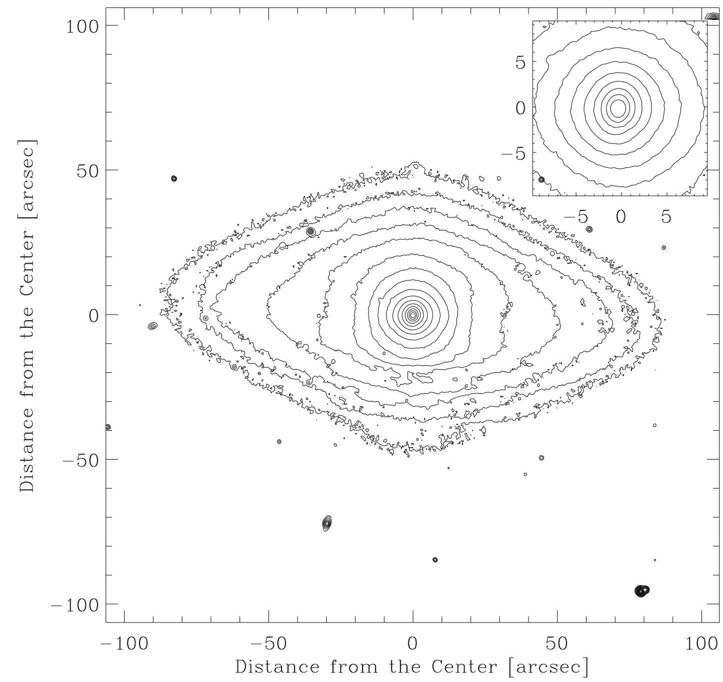

Figure 7.1: *Upper Panel:* The $R-$band isophotes of NGC 4698 (boxcar smoothed over 3×3 pixels). Isophotes are given in steps of 0.4 mag·arcsec^{-2} with the outermost one corresponding to 21.8 mag·arcsec^{-2} and the central one to 15.8 mag·arcsec^{-2}. In the *inset* the (non smoothed) isophotal map of the inner $10''$ is plotted. North is right and east up.

7.3 Results

7.3.1 Photometry

The $R-$band isophotal map of NGC 4698 is presented in Figure 7.1. A geometric decoupling (Δ P.A. $\simeq 90^\circ$) is visible both in the inner isophotes (see inset) and in the outermost one, which is characterized by two 'bumps' oriented perpendicularly to the galaxy major axis. The inner orthogonal elongation of the isophotes is more clearly visible in a F606W/WFPC2 (V-band) Hubble Space Telescope image of the same galaxy (Figure 7.2). The isophotes between $4''$ and $18''$ appear round in the plot. However as soon as an exponential disk is subtracted they also become elongated perpendicularly to the disk major axis (Figure 7.3). The overall shape of the isophotes between $18''$ and $32''$ is similar to the one observed in V (Takase, Kodaira & Okamura 1984) in B (Yasuda, Okamura & Fukugita 1995) in K' (Boselli et al. 1997) and in $K-$band (Moriondo, Giovanardi & Hunt 1998) images. This suggests that the dust does not play any role in shaping the galaxy isophotes.

We performed a bidimensional photometric decomposition of the NGC 4698 surface-brightness, which we assumed to be the sum of a $r^{1/4}$ bulge and an exponential disk. To avoid the effects of the dust lanes we performed the decomposition on the image obtained by folding the eastern side of NGC 4698 around the galaxy major axis. In performing the decomposition the seeing convolution has been taken into account. The best-fit parameters are $\mu_e = 20.4$ mag·arcsec^{-2}, $r_e = 21\farcs0$ and $q = (b/a)_{bulge} = 1.14$ (where a and b are taken along the direction of the galaxy major and minor axis respectively) for the bulge and $\mu_0 = 19.6$

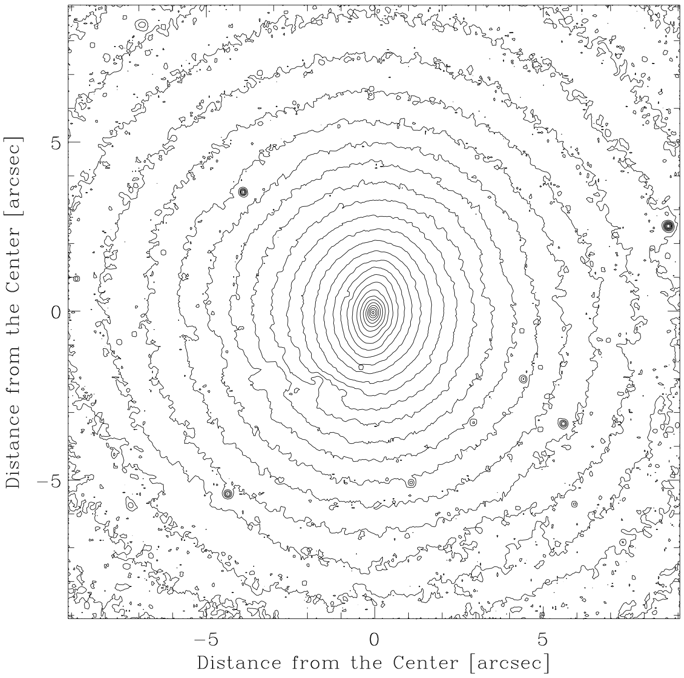

Figure 7.2: Contour plot of the very central regions of NGC 4698, with the same orientation as in Figure 7.1, as imaged with the F606W filter by the HST/WFPC2.

mag·arcsec^{-2}, $r_d = 42\farcs9$, and $i = \arccos{(b/a)_{disk}} = 65°$ for the disk. The fact that the axial ratio of the bulge is found to be greater than unity confirms the exceptional property of NGC 4698 of having a bulge elongated along the disk minor axis. The surface-brightness profiles derived along the major and minor axes of NGC 4698 and the corresponding bulge-disk decomposition are presented in Figure 7.4.

The NGC 4698 residual image obtained by subtracting the surface brightness of the exponential disk derived in the photometric decomposition is shown in Figure 7.3.

The difference between the parametric modeled and the measured surface-brightness profiles which results between $14''$ and $32''$ along the galaxy major axis (Figure 7.4) could be produced by a local fluctuation of the light distribution of the disk.

7.3.2 Kinematics

The stellar velocity curve measured along the major axis of NGC 4698 is characterized by a central plateau, indeed the stars have a zero rotation for $|r| \leq 8''$ (0.7 kpc). At larger radii the observed stellar rotation increases from zero to an approximately constant value of about 200 km s^{-1} for $|r| \gtrsim 50''$ (4.1 kpc) up to the farthest observed radius at about $80''$ (6.6 kpc). The stellar velocity dispersion profile has been measured out to $30''$ (2.5 kpc). It is peaked in the center at the value of 185 km s^{-1}. The stellar velocities measured by Corsini et al. (1999) agree within the errors with the data of this Chapter. The ionized gas kinematics along the major axis of NGC 4698 has been studied by Rubin et al. (1985) and by Corsini et al. (1999). We measured the minor-axis stellar kinematics out to about $20''$ on both sides of the galaxy. In the nucleus the stellar velocity rotation increases to about 30 km s^{-1} at $|r| \simeq 2''$. Then it decreases between $2''$ and $6''$ and it is characterized by an almost zero value

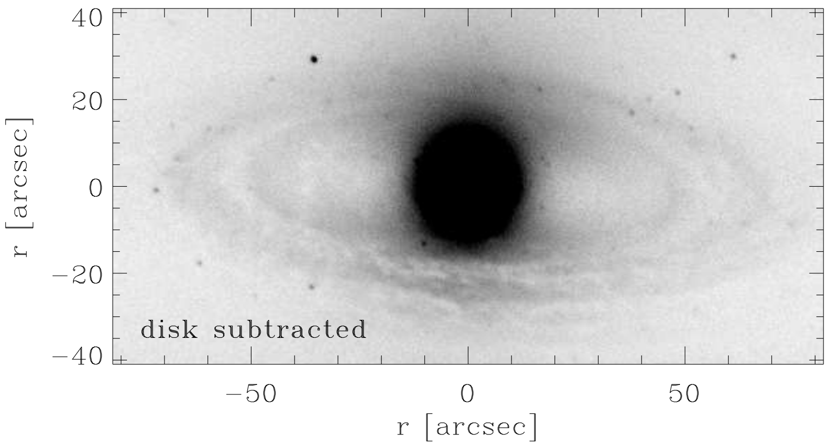

Figure 7.3: The $R-$band residual image of NGC 4698 obtained after the subtraction from the total surface-brightness distribution of the light contribution due to the exponential disk of the photometric bidimensional decomposition. North is right and east up

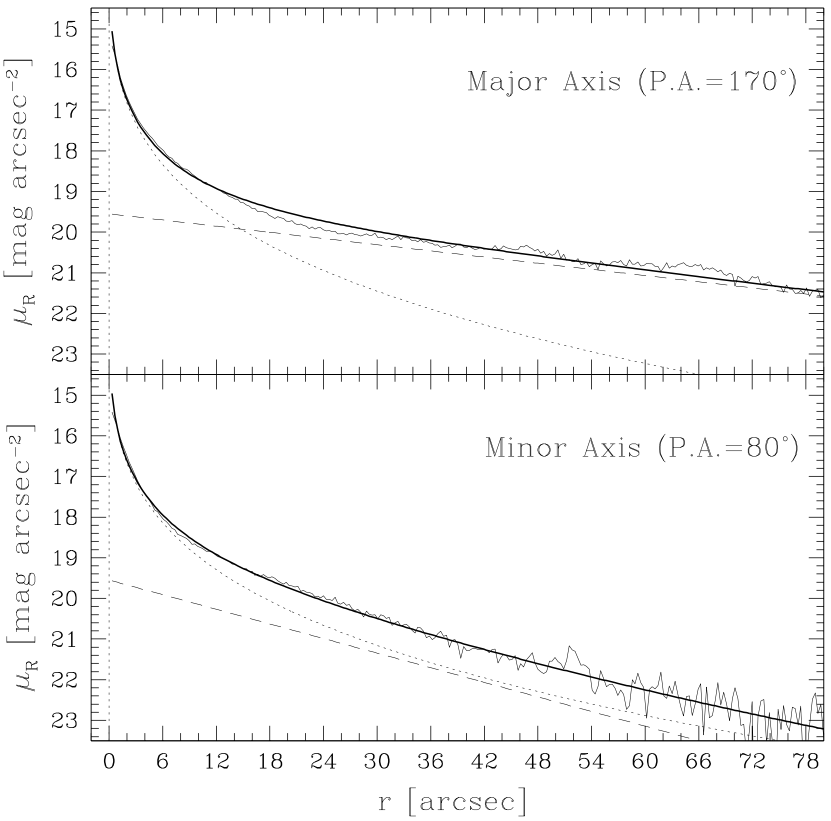

Figure 7.4: The $R-$band surface-brightness profiles of NGC 4698 (*thin continuous line*) along the major (P.A. = 170°) and minor axis (P.A. = 80°) of the galaxy out to 80″ from the center. The surface-brightness profiles of the $r^{1/4}$ bulge (*dotted line*), the exponential disk (*dashed line*) and their sum (*thick continuous line*) are also plotted

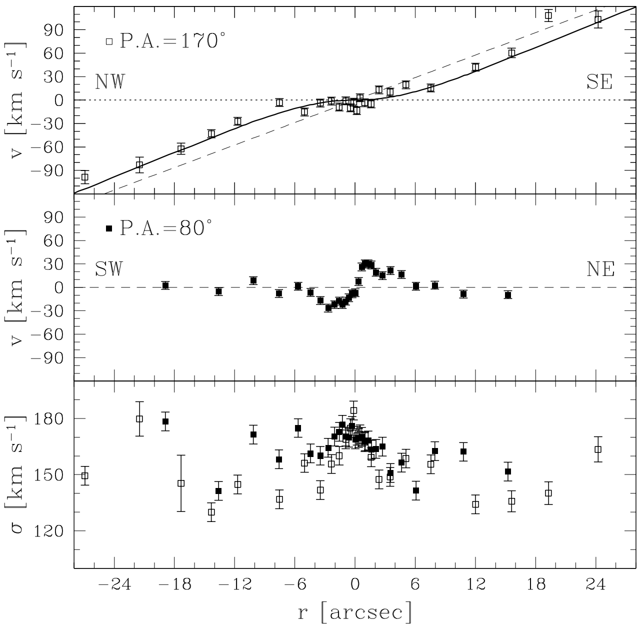

Figure 7.5: The observed stellar rotation velocity and velocity dispersion as a function of radius along the major (*open squares*) and minor axis (*filled squares*) of NGC 4698 out to $28''$ from the center. The heliocentric system velocity is $V_{\odot} = 992 \pm 10$ km s^{-1}. The *dotted* and *dashed lines* represent the velocity contribution of the bulge and disk components to the total velocity (*thick continuous line*) of our model.

beyond $6''$. The velocity dispersion profile has a central maximum of 175 km s^{-1} in agreement within the errors with the value measured along the major axis. The velocity curves and the velocity-dispersion radial profiles of the stellar component (out only to $28''$ for the spectrum along the major axis) are shown in Figure 7.5.

The spectral resolution and signal-to-noise ratio of our spectra were not sufficient to perform a two-component kinematic decomposition via double-Gaussian fit of the line-of-sight velocity distribution (LOSVD) to disentangle the contribution of bulge and disk to the observed major and minor-axis kinematics. In order to reproduce the observed velocity curve along the galaxy major axis we modeled the observed LOSVD in the following way. For the bulge we assumed a constant zero velocity and a constant velocity dispersion of $\sigma_{bulge} = 180$ km s^{-1} at all radii, while for the disk we took a velocity rising linearly to match the outer points of the plotted curve (where the light contribution of the bulge is negligible) with a constant velocity dispersion of $\sigma_{disk} = 100$ km s^{-1}. The resulting velocity curve obtained by fitting with a Gaussian the sum of the two Gaussian components of bulge and disk weighted according to the photometric decomposition of Figure 7.4 is shown with a continuous line in the upper panel of Figure 7.5. The agreement with the observed points is good. In particular the flat central part of the observed velocity curve is well reproduced. For $|r| > 50''$ the bulge contribution to the galaxy light is negligible and the constant stellar rotation ($V \simeq 200$ km s^{-1}) we measure out to $80''$ can be directly explained by the differential rotation of the disk.

As far as the kinematics along the minor axis is concerned, the observed radial velocities and velocity dispersions are to be ascribed mainly to the bulge component, which dominates over the disk at all radii. It results that the rotation of the bulge is mainly limited to the central region. For $|r| > 6''$ the lack of detailed information about the shape of the LOSVD prevents us to detect even a small overall rotation of the bulge, in spite of what one would expect considering the elongated shape of its isophotes. Therefore it is reasonable to ascribe to the entire bulge a projected angular momentum perpendicular to that of the disk.

7.4 Discussion and conclusion

7.4.1 The bulge-disk decoupling scenario

In the previous paragraph adopting a parametric photometric decomposition, we have pointed out that the bulge and disk of the Sa NGC 4698 appear on the sky elongated perpendicularly to each other and characterized by the rotation around two orthogonal axes. Assuming that the intrinsic shape of bulges is generally triaxial (Bertola, Vietri & Zeilinger 1991) and that the plane of the disk coincides with the plane perpendicular either to the bulge major or minor axis, we deduce from the observed configuration that the major axis of the bulge is perpendicular to the disk, given that the latter is seen not far from edge on. The fact that the velocity field of the bulge is characterized by a zero velocity along its apparent minor axis (as indicated by the central plateau in the rotation curve along the disk major axis) and by a velocity gradient along its major axis suggests that the rotation axis of the bulge lies on the plane of the disk, and therefore the intrinsic angular momenta of bulge and disk are perpendicular.

The orthogonal decoupling of the bulge and disk in NGC 4698 indicates that a second event occurred in the formation history of this galaxy. We suggest that the disk has formed at a later stage due to the acquisition of material by a triaxial spheroid on its principal plane perpendicular to the major axis. An example of acquisition on the plane perpendicular to the minor axis could be represented by NGC 7331 (Prada et al. 1996), where the bulge has been found counterrotating with respect to the disk (although this result has been recently questioned by Bottema 1999). Up to now NGC 4698 and NGC 7331 represent the only cases of kinematic evidence that disk galaxies with prominent bulges could be started as 'undressed spheroids' and their disks accreted gradually over several billion years, as suggested by Binney & May (1986). Recently such kind of processes have been considered within semi-analytical modeling techniques for galaxy formation, where the disks accrete around bare spheroids previously formed either directly from the relaxation of gas in a spherical distribution parallel to that of their surrounding dark halos (Kauffmann 1996), or from the merging of disk protogalaxies previously formed (Baugh, Cole & Frenk 1996). In this framework we could expect that the shape of the dark matter halo of NGC 4698 correlates with that of the pre-existing galaxy (namely the actual bulge) as in the case of the prototype polar-ring galaxy NGC 4650A. In this galaxy Sackett et al. (1994) found a highly flattened dark halo, which has the same orientation of the pre-existing S0 rather than that of the acquired gaseous ring. If the disk of NGC 4698 has an external origin then polar-ring elliptical galaxies like NGC 5266 (Varnas et al. 1987) and AM 2020-504 (Whitmore et al. 1990) and ellipticals with dust lane along the minor axis (Bertola 1987) could represent transient stages towards the formation of spiral systems like NGC 4698.

The possible presence of an end-on bar lying in the plane of the disk is ruled out since we measure along the major axis a zero-velocity plateau instead of a strong velocity gradient similar to those predicted by Merrifield (1996) for end-on bars in edge-on galaxies.

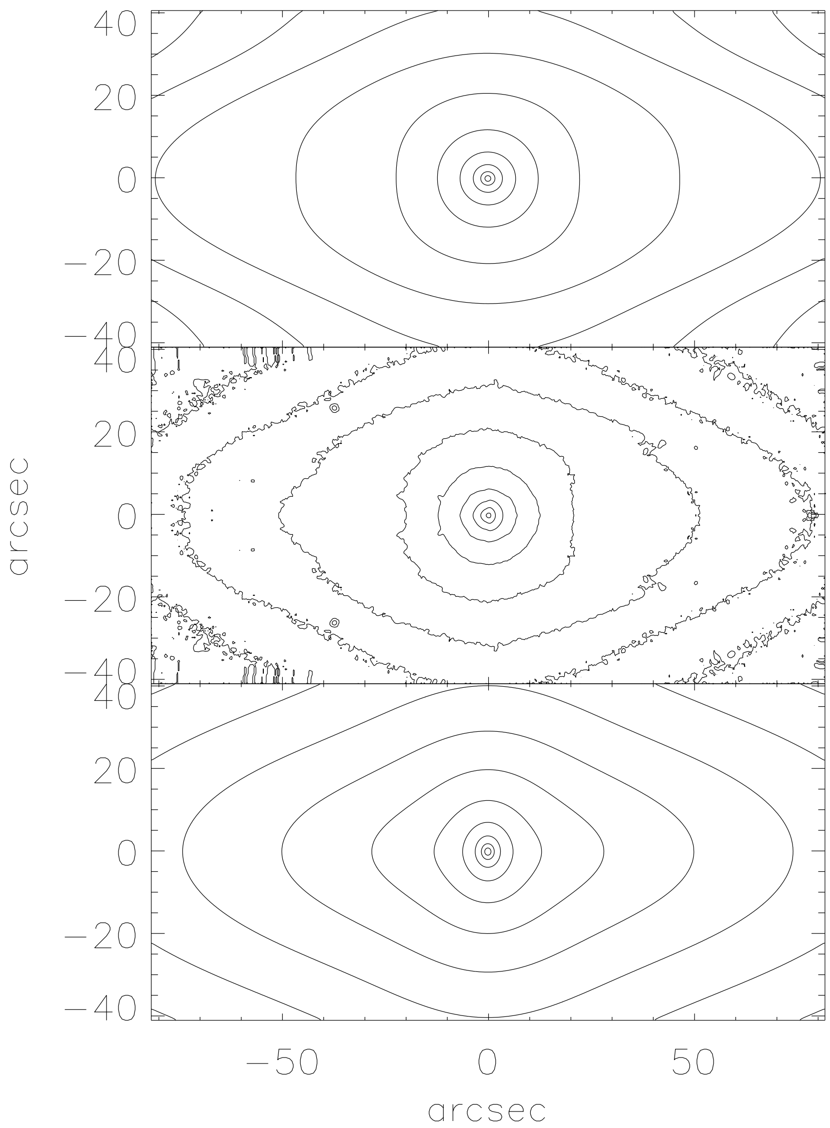

Figure 7.6: This plot demonstrates the importance of using a non-parametric bulge-disk decomposition to determine the geometric parameters of disk and bulge. The *Middle Panel* presents a logarithmically spaced contour plot of an R-band image of the Sa galaxy NGC 4698 (folded with respect to the major axis to limit the effects of dust lanes in front of the bulge). The *Upper Panel* shows the same contour plot for a non-parametric photometric model of this galaxy. The *Bottom Panel* presents the best fitting 2D parametric model (exponential + $r^{1/n}$) of the same galaxy. It is apparent that the best parametric model completely misses the main characteristics of this galaxy photometry. In particular the rather boxy shape of the bulge is well reproduced in the upper panel *non-parametric* model, but is *not* reproduced by the bottom panel *parametric* model. Note that the same surface brightness levels have been used in all three plots.

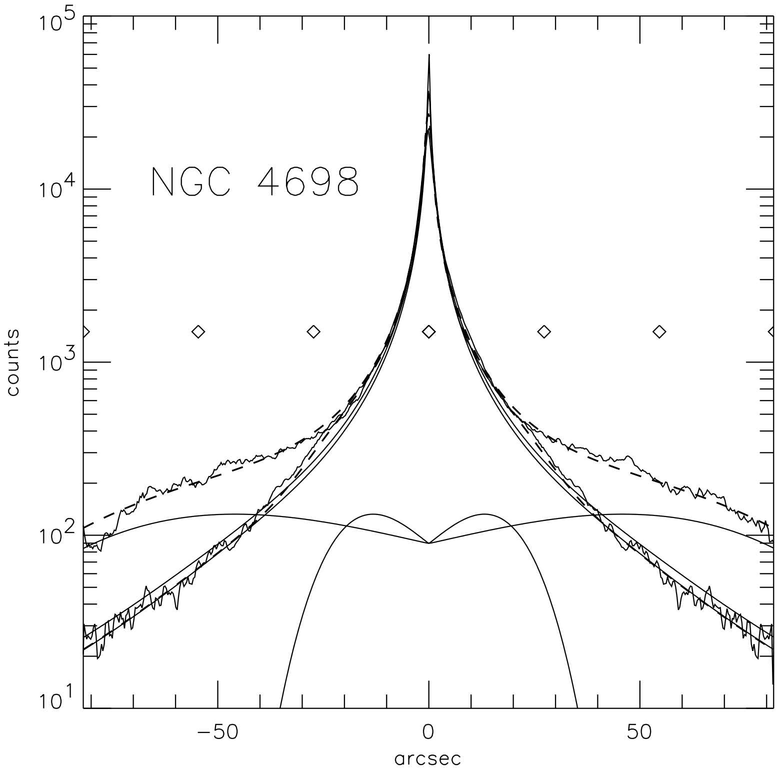

Figure 7.7: Non-parametric disk-bulge decomposition for NGC 4698: the disk and the bulge are constrained to have elliptical isophotes with constant ellipticity and position angle, but no functional form is imposed to the profiles. We show here two cuts, both along the major and minor axis, of the observed galaxy (solid noisy line) and of the non-parametric model (dashed line). The best fitting non-parametric disk is represented by the solid lines that decreases toward the center.

7.4.2 An alternative scenario

A non-parametric photometric decomposition of the NGC 4698 surface-brightness distribution has been recently proposed by Moriondo et al. (1998). The resulting bulge shows circular isophotes and it dominates the galaxy light out to about $20''$ from the center along the galaxy major axis, the surface-brightness profile of the disk flattens in the inner $30''$.

We have developed a modified algorithm based on the same general idea that the only constraint given to both the bulge and the disk is that they have constant ellipticity and position angle. Only this decomposition is able to provide a good fit to the photometry and in particular is able to reproduce in detail the peculiar characteristic shape of the NGC 4698 isophotes. A comparison between the observed isophotes, the best fitting parametric fit and the non-parametric one is shown in Figure 7.6. The profiles of the best fitting non-parametric bulge-disk decomposition are shown in Figure 7.7.

The disk light contribution becomes so small for $|r| < 30''$ along the major axis that the rotation we observe has to be attributed mainly to the bulge component, which indeed would rotate in the same sense of the disk. In order to explain the central plateau along the disk major axis, the velocity gradient and the elongation of the inner isophotes along the disk minor axis it is necessary to assume the presence of a third luminous component in the central region of NGC 4698 in addition to the round bulge and the disk with a flattened surface-brightness profile. It should be noted that in the statistics of Bertola et al. (1991) round bulges (as well as those perpendicular to the disk) are not present.

If we adopt the non-parametric photometric decomposition we are lead to conceive the presence in the center of NGC 4698 of a structure similar to that of the kinematically decoupled cores observed in several ellipticals (see Mehlert et al. 1998 for a list). In ellipticals isolated cores generally tend to not show up photometrically (de Zeeuw & Franx 1991) while the isophotes of the NGC 4698 core is characterized by an orthogonal geometric decoupling with respect to those of the disk. Therefore the core in NGC 4698 (which should be the first case of an isolated core observed in a spiral galaxy) is photometrically decoupled from the disk and kinematically decoupled with respect to both bulge and disk. Also according to this alternative scenario NGC 4698 experienced a second event in its history.

Bibliography

Baugh, C.M., Cole, S., Frenk, C.S. 1996, MNRAS, 283, 1361

Bender, R. 1990, A&A, 229, 441

Bertola, F. 1987, In: Structure and Dynamics of Elliptical Galaxies, T. de Zeeuw (ed.), Reidel, Dordrecht, p. 135

Bertola, F., Vietri, M., Zeilinger, W.W. 1991, ApJ, 374, L13

Bertola, F., Cinzano, P., Corsini, E.M., Pizzella, A., Persic, M., Salucci, P. 1996, ApJ, 458, L67

Binney, J.J., May, A. 1986, MNRAS, 218, 743

Boselli, A., Tuffs, R.J., Gavazzi, G., Hippelein, H., Pierini, D. 1997, A&AS, 121, 507

Bottema, R. 1999, A&A, submitted [astro-ph/9902240]

Corsini, E.M., Pizzella, A., Sarzi, M., Cinzano, P., Vega Beltrán, J.C., Funes, J.G., Bertola, F., Persic, M., Salucci, P. 1999, A&A, 342, 671

de Vaucouleurs, G., de Vaucouleurs, A., Corwin Jr., H.G., Buta, R.J., Paturel, G., Fouquè, P. 1991, Third Reference Catalogue of Bright Galaxies, Springer-Verlag, New York (RC3)

de Zeeuw, T., Franx, F. 1991, ARA&A, 29, 239

Freedman, W.L., Madore, B.F., Mould, J.R., Ferrarese, L., Hill, R., Kennicutt Jr., R.C., Saha, A., Stetson, P.B., Graham, J.A., Ford, H., Hoessel, J.G., Huchra, J., Hughes, S.M., Illingworth, G.D 1994, Nature, 371, 757

Kauffmann, G. 1996, MNRAS, 281, 487

Mehlert, D., Saglia, R.P., Bender, R., Wegner, G. 1998, A&A, 332, 33

Merrifield, M.R. 1996, In: Barred galaxies, Buta, R.D., Crocker, D.A., Elmegreen, B.G. (eds.), ASP Conf. Ser. 91, ASP, San Francisco, p. 176

Moriondo, G., Giovanardi, C., Hunt, L.K. 1998, A&AS, 130, 81

Prada, F., Gutierrez, C.M., Peletier, R.F., McKeith, C.D. 1996, ApJ, 463, L9

Rubin, V.C., Burstein, D., Ford Jr., W.K., Thonnard, N. 1985, ApJ, 289, 81

Sackett, P.D., Rix, H.-W., Jarvis, B.J., Freeman, K.C. 1994, ApJ, 436, 629

Sandage, A., Bedke, J. 1994, The Carnagie Atlas of Galaxies, Carnagie Institution, Flintridge Foundation, Washington (CAG)

Sandage, A., Tammann, G.A. 1981, A Revised Shapley-Ames Catalog of Bright Galaxies, Carnagie Institution, Washington

Schröeder, A., Visvanathan, N. 1996, A&AS, 118, 441

Takase, B., Kodaira, K., Okamura, S. 1984, An Atlas of Selected Galaxies, Tokyo University Press, Tokyo

Varnas, S.R., Bertola, F., Galletta, G., Freeman, K.C., Carter, D. 1987, ApJ, 313, 69

Whitmore, B.C., Lucas, R.A., McElroy, D.B., Steiman-Cameron, T.Y., Sackett, P.D., Olling, R.P. 1990, AJ, 100, 1489

Yasuda, N., Okamura, S., Fukugita, M. 1995, ApJS, 96, 359